ORGANIC PROCESS RESEARCH & DEVELOPMENT
OPR&D

pubs.acs.org/OPRD
Article

Nonclogging Liquid-Walled Continuous Flow Reactors

Alejandro Mata, Caroline de Fraipont, Céline Hervieux, Lucas Giacchetti, Oicime Hadj-Sassi, Alexandra Bogicevic, Vincent Marichez,* and Thomas M. Hermans*

Cite This: *Org. Process Res. Dev.* 2025, 29, 472−478
Read Online
ACCESS | Metrics & More | Article Recommendations | Supporting Information

ABSTRACT: Flow chemistry is rapidly growing as it can outperform batch processes in terms of production costs, product quality, and overall environmental footprint. However, the reaction scope in flow is currently restricted due to solid handling limitations. Solids such as heterogeneous catalysts (powders) or precipitates are known to clog flow reactors, leading to periods of downtime to clean (or sometimes even replace) the reactor. Here, we report on liquid-walled continuous flow reactors that are virtually insensitive to clogging (or abrasion) and mix an order of magnitude faster than do solid-wall analogs. Our walls consist of chemically inert ferrofluids that are held in place with permanent magnets, leading to a stable liquid−liquid interface. We show efficient formylation of aryl bromides that is normally plagued by in-line precipitation.

KEYWORDS: *flow chemistry, clogging, mixing, formylation*

1. INTRODUCTION

Flow chemistry offers numerous advantages over batch processes in selected cases,[1] such as (i) uninterrupted production—no downtime due to emptying/cleaning sessions, (ii) smaller footprint,[2] (iii) lower solvent consumption—a 10-fold reduction,[3] crucial since 50% of the resource usage (and GHG emissions) in API processes is due to organic solvents,[4,5] (iv) better quality due to an overall better control over the reaction parameters such as thermal and mass transfer,[6,7] and (v) improved safety.[8] Flow chemistry therefore leads to a drastic reduction in the production costs (significant OPEX reduction) as well as a lower environmental footprint.[2,3] However, despite the clear assets of continuous flow techniques, batch processes remain dominant among fine chemical and pharmaceutical industrials.[9] One of the main reasons is the narrow application scope offered by continuous flow reactors as they cannot handle solids—ubiquitous in chemistry—without clogging or breaking. In fact, Lonza shared that among 80 API chemical processes, about 50% could greatly benefit from a batch to flow transposition, but 2/3rd cannot be performed into flow reactors due to solid handling difficulties (ranging from in-line precipitation to resorting to heterogeneous catalysts).[9] In this context, many efforts have been made to find a way around this technical limitation, such as using slug flows,[10] applying sonication,[11] oscillatory flows,[12] or cascades of continuous stirred-tank reactors,[13,14] to prevent blockage of the equipment. However, these solutions remain either impractical at the industrial scale (costly, unscalable, etc.) or limited in terms of acceptable solid content. Here, we show liquid-walled continuous flow reactors capable of handling chemical slurries by flowing the reaction media through an immiscible ferrofluid jacket that is held in place by a simple quadrupolar magnetic field (see Figure 1a−c).[15−17]

Previously, we have shown how diamagnetic liquids can be magnetically levitated by immiscible ferrofluids in quadrupolar magnetic fields.[15] Briefly, 4 permanent NdFeB magnets are positioned as shown in Figure 1a, resulting in a theoretical magnetic null-line at the center of the gap (between the magnets) and extending over the entire length of the reactor. Emanating outward from the null-line are increasingly high magnetic field values ranging up to ∼0.5 T. When injecting a ferrofluid, it occupies the high-field zone, whereas diamagnetic liquids are pushed to the null-line. The ferrofluid remains in the reactor at all times because it is magnetically attracted. In effect, this creates "liquid tubes" of the diamagnetic liquid surrounded by a ferrofluid jacket. Liquid tubes have unique properties such as 60−90% reduced drag,[18] plug flow depending on the ratio of viscosities of the flowing media and that of the ferrofluid,[19] and ultrasoft walls (2−10 kPa).[20] Liquid tube diameters can range from μm to cm,[19] and lengths of 1 m have been demonstrated.[15] The liquid walls can easily deform to adapt to the shape of any solid aggregate and evacuate it in a nearly frictionless manner.[15,18] This grants the liquid tube technology unique solid handling capabilities, thus unlocking previously impossible continuous flow processes such as heterogeneous catalysis or crystallization/precipitation without clogging issues or production downtime.

2. MIXING TIME CHARACTERIZATION

Other than solid handling, a second requirement for efficient reactors is good mass transfer. Indeed, fast mixing is key in numerous continuous flow processes to ensure high yield and selectivity, e.g., flash chemistry,[21] a widespread powerful toolbox in chemical and pharmaceutical industries known to involve

Received: October 25, 2024
Revised: January 27, 2025
Accepted: January 30, 2025
Published: February 12, 2025

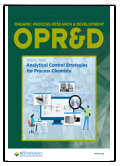

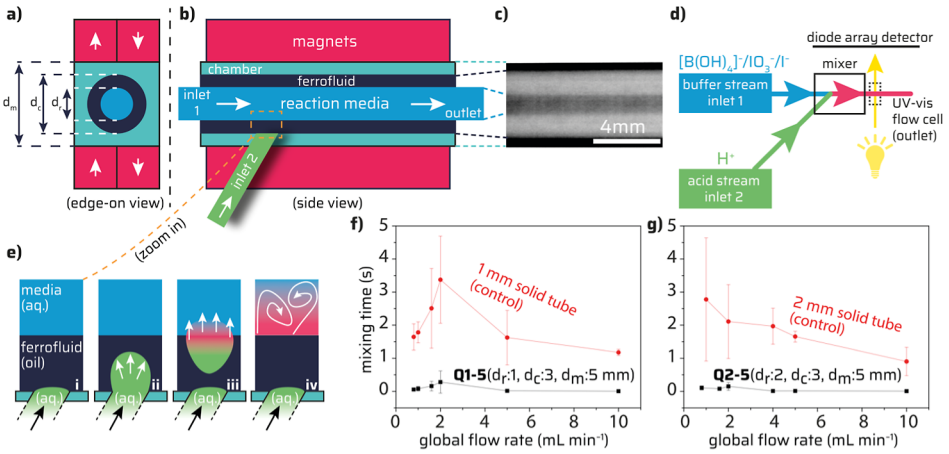

Figure 1. : Flow behavior and mixing in a liquid-walled reactor. (a) Schematic edge-on and side views of a typical reactor with control over the diameters of the reaction media (d_r), chamber (d_c), and magnet distance (d_m). The quadrupolar magnet arrangement ensures a null magnetic field line in the reaction media along the flow direction. (b) Multiple additional inlets (here, one shown in green) can be inserted, whose flow traverses the ferrofluid to access the reaction media. (c) X-ray transmission image of a 1 mm diameter liquid tube of water inside a silicon-based ferrofluid (MFS 6022 from Magron). (d) Schematic layout of the setup to quantify mixing time using the Villermaux–Dushman reaction. (e) Rapid mixing of the acid stream (green) and buffer stream (blue). (i–ii) The ferrofluid layer forces the acid stream to form droplets, which are (iii) accelerated toward the center of the liquid tube due to diamagnetic repulsion, (iv) leading to eddies and mixing. (f,g) Mixing times quantification (at least $n = 3$, error bars show standard deviations) for 1 and 2 mm diameter tubes; length is 50 mm for both (d_r, d_c, and d_m are defined in panel a). Solid-wall controls were 3D printed to match the geometry (angle of inlet 2) and the dimensions of the corresponding liquid-walled reactor. The exact dimensions of both the reactors and their respective controls are in Figures S4 and S5.

highly reactive species. We therefore quantified the mixing times of our reactors using the (gold-standard) Villermaux–Dushman reaction used by the flow community.[22−24] It consists of 2 parallel competitive reactions including an acid–base reaction in a borate buffer (eq 1) and an iodine–iodate reaction (eq 2), yielding iodide that further reacts with iodine ions to yield triiodide ions (eq 3), which can be photometrically detected using UV–vis spectrometry (at 353 nm).

$$B(OH)_4^- + H^+ \xrightarrow{k_1} B(OH)_3 + H_2O \tag{1}$$

$$5I^- + IO_3^- + 6H^+ \xrightarrow{k_2} 3I_2 + 3H_2O \tag{2}$$

$$I_2 + I^- \underset{k_3'}{\overset{k_3}{\rightleftharpoons}} I_3^- \tag{3}$$

where k_1, k_2, k_3, and k_3' are the reaction rate constants. Since Reaction 1 is considered instantaneous, in the case of a perfect mixing, it will be dominant, and triiodide will thus not be formed. In the case of poor mixing, local pockets of acid will yield the formation of triiodide (since both reactions can then occur simultaneously). In short, it is possible, thanks to recent contributions,[24] to characterize the mixing efficiency of any reactor by recording the UV–vis absorption signal at 353 nm when mixing 2 streams inside the reactor (acid and borate buffer, see green and blue in Figure 1d, respectively).

The volume V_2 (for the acid stream) can be described as its initial value modified by the incorporation of the volume V_1 (for the borate buffer stream), where $g(t)$ is called the incorporation function (eq 4).

$$V_2(t) = V_{2,0} + V_{1,0}g(t) \tag{4}$$

The evolution of the quantity of each species can therefore be derived as follows (n in moles)

$$\frac{dn_{H^+}}{dt} = -r_1 - 6r_2 \tag{5}$$

$$\frac{dn_{I^-}}{dt} = n_{I_0^-}\frac{dg}{dt} - 5r_2 - r_3 \tag{6}$$

$$\frac{dn_{IO_3^-}}{dt} = n_{IO_{3,0}^-}\frac{dg}{dt} - r_2 \tag{7}$$

$$\frac{dn_{I_2}}{dt} = 3r_2 - r_3 \tag{8}$$

$$\frac{dn_{I_3^-}}{dt} = r_3 \tag{9}$$

$$\frac{dn_{H_2BO_3^-}}{dt} = n_{H_2BO_{3,0}^-}\frac{dg}{dt} - r_1 \tag{10}$$

$$\frac{dn_{H_3BO_3}}{dt} = n_{H_3BO_{3,0}}\frac{dg}{dt} + r_1 \tag{11}$$

where r_1, r_2, and r_3 are the reaction rates of the Villermaux–Dushman reaction (see eqs 1–3), where the linear incorporation function $g(t)$ is defined as

$$g(t) = t/t_m \tag{12}$$

where t_m is the characteristic mixing time of the device.

By solving this set of equations, one can access, by fixing a t_m value, the corresponding segregation index of any system (see eq 13).

$$X_S = \frac{2(n_{I_2} + n_{I_3^-})}{n_{H_0^+}} \cdot \frac{6n_{IO_{3,0}^-} + n_{H_2BO_{3,0}^-}}{6n_{IO_{3,0}^-}} \tag{13}$$

One can then plot the mixing time as a function of the segregation index and use this as a tool to access mixing times of any reactor based on the experimental segregation index values calculated from the initial conditions and the extracted UV–vis signal (directly accounting for the concentration of I_3^- anions).

https://doi.org/10.1021/acs.oprd.4c00459
Org. Process Res. Dev. 2025, 29, 472−478

Scheme 1. Formation of Solid LiOH (Insoluble in THF) When Traces of Water Are Present

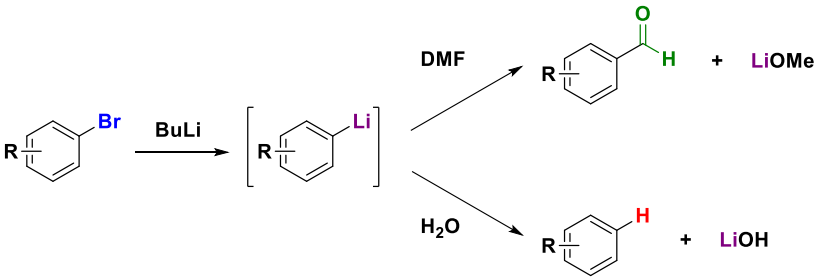

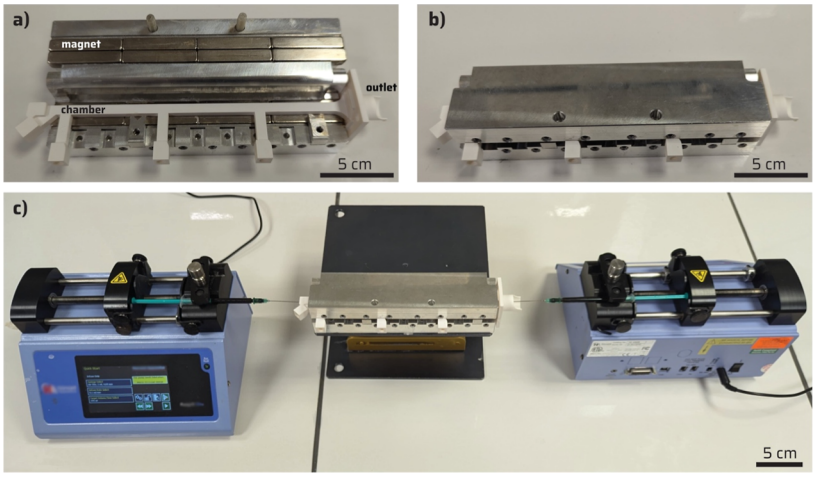

Figure 2. (a) 3D-printed chamber (3 mm I.D., 20 cm shown in white) on an opened magnet holder consisting of 16 bar magnets. See Figure S5 for a large technical drawing of the chamber with exact dimensions. (b) Chamber held inside the closed magnetic frame. The attraction of the magnets in the quadrupolar arrangement ensures that the holder stays firmly closed. (c) Two syringe pumps inject ferrofluid inside the chamber until 2 mm I.D. of the THF phase is reached (verified by X-ray transmission imaging, see Supporting Information Section 2.3).

Table 1. System Setup and Optimization of the Formylation of Aryl Bromides in a Liquid-Walled Reactor under Continuous Flow Conditions[a]

a)

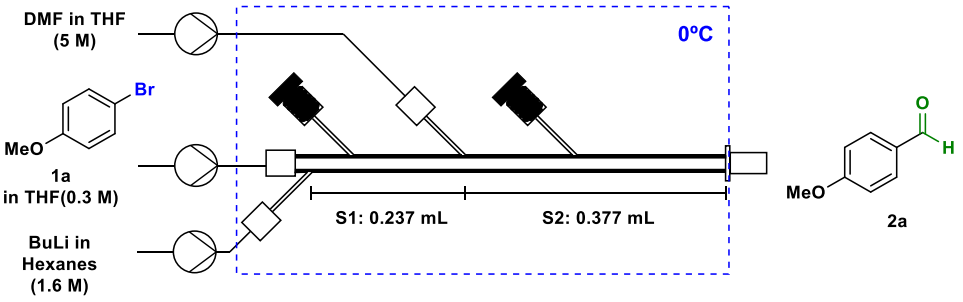

b)

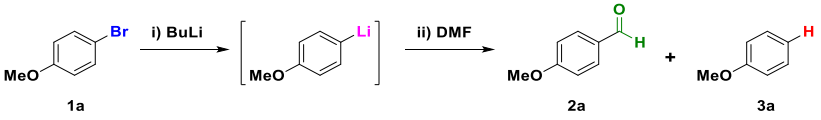

entry	BuLi equiv.	DMF equiv.	S1 residence time	S2 residence time	yield[b] (%)
1	1.6	5	30 s	37 s	56
2	1.6	5	60 s	74 s	67
3	2	6.25	60 s	74 s	71
4[c]	2	6.25	60 s	74 s	71

[a]Reaction conditions: 4-bromoanisole **1a** (3 mmol) in THF (10 mL), commercial solution of butyl lithium in hexanes (1.6 M), DMF (2.5 mmol) in THF (5 mL); the outcome of the reactor was collected over water. Temperature: 0 °C. [b]Yields were determined by ^{1}H NMR analysis of the crude mixture after workup. In all cases, less than 5% of side product anisole **3a** was detected. [c]Reactions done in solid tubes (see Supporting Information Section 1.5 for the reactor setup).

https://doi.org/10.1021/acs.oprd.4c00459
Org. Process Res. Dev. 2025, 29, 472−478

Scheme 2. Substrate Scope of Benzaldehydes Synthesized by the Developed Continuous Flow Protocol in a Liquid-Walled Reactor[a]

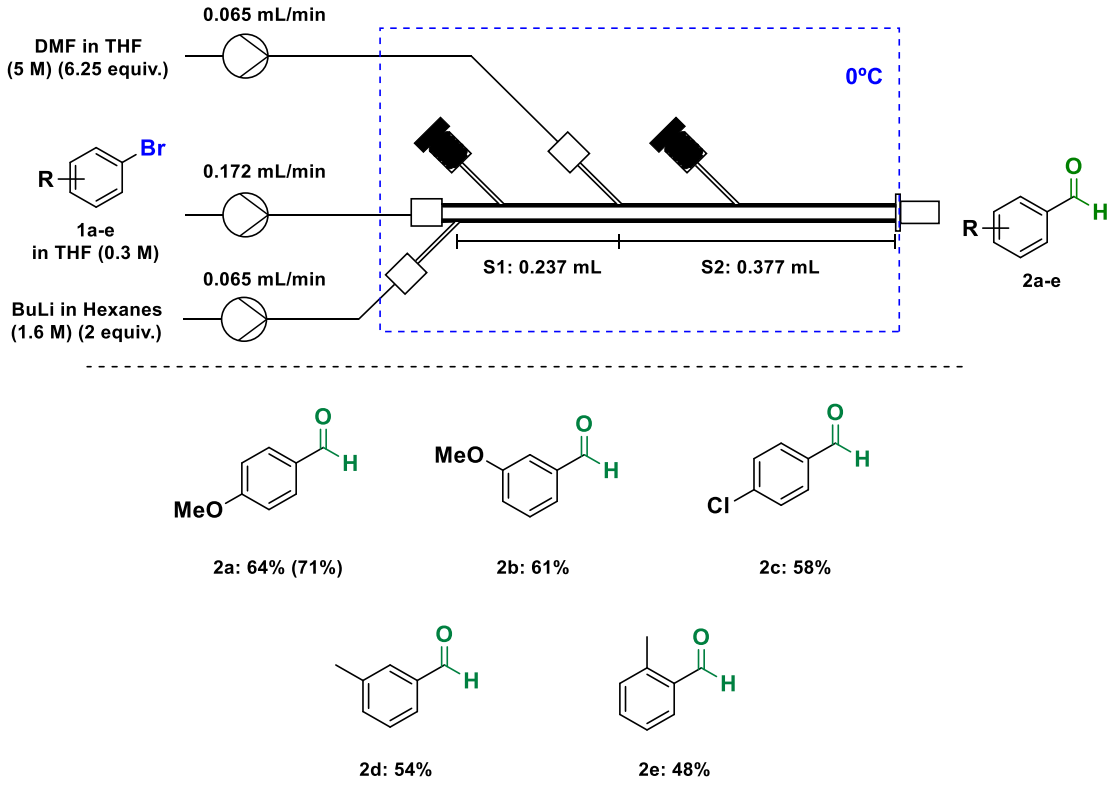

[a]Yields shown are the isolated products after column chromatography purification. The value in parentheses denotes the ^{1}H NMR yield of the crude after workup.

We found that rapid mixing is only achieved when inlet 2 is positioned below the ferrofluid layer, that is, the acid (aqueous) phase needs to traverse the oily ferrofluid layer (cf. the orange dashed box in Figure 1b). The oily ferrofluid acts as a droplet generator, but upon (acid) droplet formation, a high diamagnetic repulsion is exerted, resulting in rapid merging and mixing with the borate buffer stream (Figure 1e). The droplet generation at inlet 2 and its expulsion into the main channel (coming from inlet 1) was visualized by high-speed high-resolution X-ray radiology (see Video S1). Due to this "forced droplet merging" effect, the mixing times in our devices are about 1 order of magnitude better than those in solid-wall analogs (Figure 1f,g). Specifically, in **Q1−5**, we achieve 56 ± 38 and 6 ± 1 ms at, respectively, 0.8 and 10 mL min^{-1}. For **Q2−5**, we obtained 107 ± 63 and 6 ± 3 ms at 0.8 and 10 mL min^{-1}, respectively. As a comparison, standard T-micromixers typically have mixing times 1 order of magnitude higher.[25] In addition, compared to their solid-walled control, the mixing efficiency of the liquid-walled reactors is nearly independent of the flow rate (Figure 1f,g). Static mixers can provide good mixing times but often suffer from poor solid handling.[26,27]

To illustrate the need for a reliable flow reactor capable of solid handling, Kappé's group described the formation of peptides via the azide method in continuous flow.[28] In their work, the precipitation of intermediates in the aqueous media forced—through repeated clogging issues—the use of an organic cosolvent. The latter cosolvent addition did permit the translation of the process to continuous flow, thus addressing the safety issues of this method in batch operation. However, lower yields were achieved, and the substrate scope was reduced compared to that of the process using only water as solvent.

3. CHEMISTRY BENCHMARK (FORMYLATION OF ARYL BROMIDES)

Having shown efficient mixing and solid handling, we demonstrate the liquid-walled reactor performance on formylation of aryl bromides using a lithium organometallic base since it requires fast mixing to avoid hot spots or concentration differences.[29] Moreover, both the reagents and intermediates require a strictly dry environment to prevent side reactions and production of solid LiOH (see the bottom pathway in Scheme 1), which clogs traditional flow reactors.[30]

The liquid-walled reactor consists of a 3D-printed chamber (20 cm long, 3 mm I.D.; see Figure S5 for detailed technical drawings) placed inside an aluminum frame with NdFeB magnets (Figure 2a). The lid of the frame is then closed (Figure 2b), thus forming quadrupolar magnetic fields around the chamber. Ferrofluid (0.78 mL) is injected using two syringe pumps (Harvard Apparatus, Pump 11 Elite) at 0.1 mL min^{-1}. To ensure an even distribution of the ferrofluid throughout the chamber, the ferrofluid was introduced in four 0.195 mL injections (one per magnet) with the tip of each syringe aligned with the middle of the corresponding magnet (Figure 2c). Finally, the system was equilibrated by flowing tetrahydrofuran (THF) for 30 min through the inlets at the flow rates that are to be used in the reactions.

The flow system, see Table 1a, was assembled consisting of the above explained liquid-walled reactor, a peristaltic pump, and two syringe pumps. To set the temperature to 0 °C, the

https://doi.org/10.1021/acs.oprd.4c00459
Org. Process Res. Dev. 2025, 29, 472−478

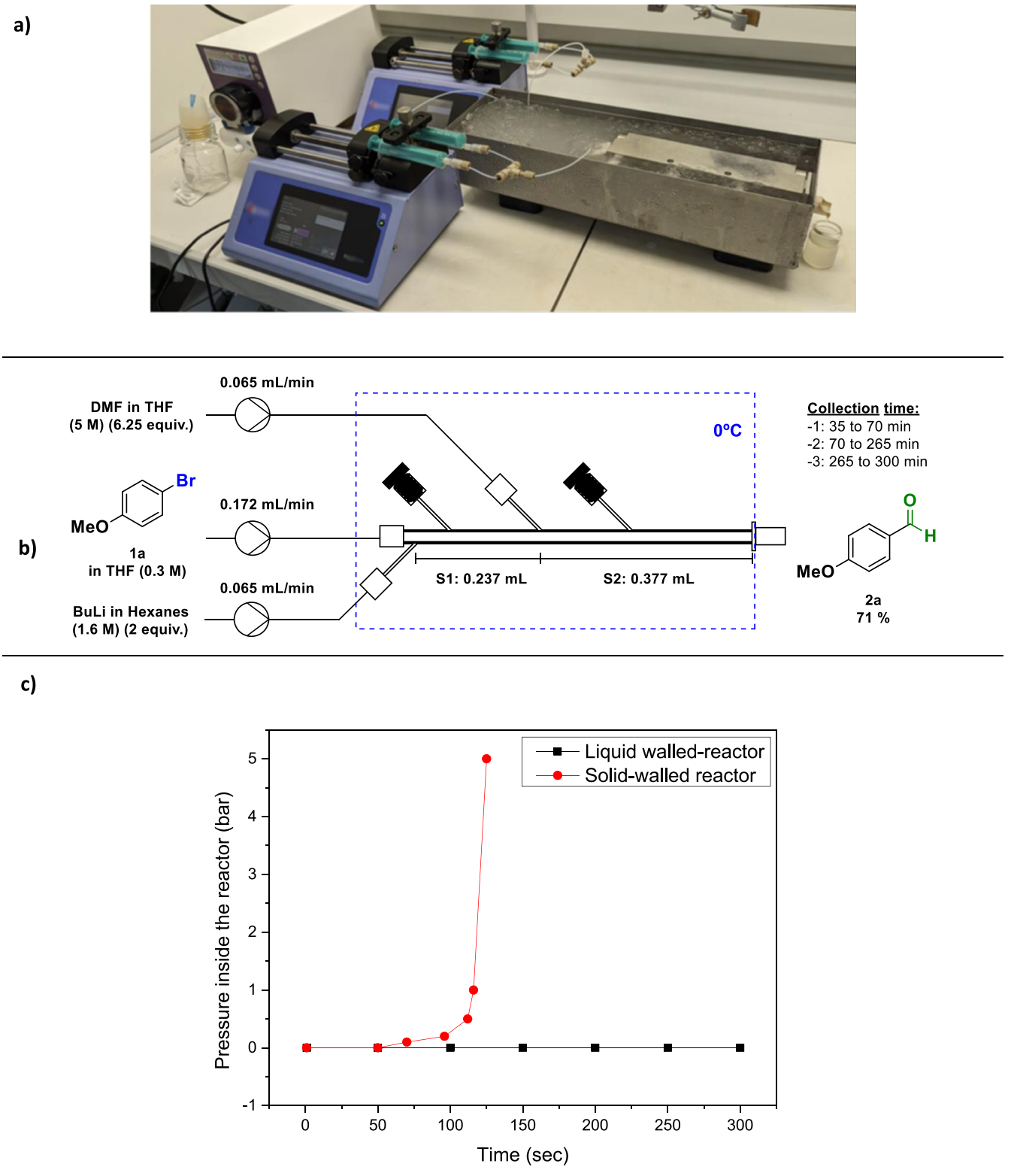

Figure 3. Scale-out processing of the developed protocol. Yield was determined by ^{1}H NMR analysis of the crude after workup. (a) Picture of the reactor. (b) Reaction scheme and conditions used. (c) Comparison of the evolution of pressure between liquid tube and solid tube processing, highlighting the nonclogging asset of the liquid-walled reactor (no downtime).

chamber was submerged in an ice bath. The distribution of the three inlets formed 2 different reactor sections in the liquid tube reactor. In reactor section S1, the first two inlets introduce the starting material solution and the butyl lithium solution, resulting in the lithiation of the aryl bromide substrate. Then, the addition of dimethylformamide (DMF) in THF solution allows the formylation in reactor S2, thus completing the reaction sequence. *n*-Butyl lithium is a highly reactive and pyrophoric compound; it must be handled under an inert atmosphere (e.g., argon or nitrogen) and with appropriate

https://doi.org/10.1021/acs.oprd.4c00459
Org. Process Res. Dev. 2025, 29, 472−478

personal protective equipment, including flame-resistant lab coats, chemical-resistant gloves, and safety goggles, to prevent exposure and mitigate fire hazards.

As a model substrate (Table 1b), 4-bromoanisole (**1a**) was used, yielding 4-methoxybenzaldehyde (**2a**) as the desired product. To hard-test the solid handling capabilities of the liquid reactor, high-performance liquid chromatography quality (non-dry) THF was used to increase the production of solids inside the reactor. A screening campaign was undertaken, see Table 1, to identify if high yields could be obtained when applying such a relatively high-water-content solvent. A promising first result (entry 1) was obtained, providing a moderate 56% yield. By doubling the reaction times and increasing the equivalents of both reagents (entries 2 and 3), a good yield of 71% was achieved. Interestingly, despite use of nondry solvent, a very low presence (<5%) of side product **3a** was observed in all experiments. To demonstrate the chemical inertness of the ferrofluid layer used in the liquid-walled reactor, we performed a control reaction at short run times (<60 min) before clogging could occur in solid-walled tubes. Virtually identical results (entries 3 and 4) were obtained using either the liquid-walled reactor or a solid-walled reactor as a control. This observation, especially for such a sensitive reaction and involving highly reactive reagents, strongly indicates that the ferrofluid does not interfere with the reaction media.

Using the optimal conditions explained above, the substrate scope was extended to determine the applicability of this method to other aryl bromides (Scheme 2). Several electron-neutral and electron-rich benzaldehydes were successfully obtained from the corresponding aryl bromides after column chromatography purification in moderate yields.

In order to demonstrate the benefits of liquid tube technology for organolithium reactions, scale-out experiments using the model substrate were performed (Figure 3a,b). This involved 55 mL of starting material solution (300 min processing time), using the previous optimal conditions (Table 1—Entry 3). To determine the stability of the reactor over time, the collection was split into 3 different stages during the run. Gratifyingly, 71% yield was observed by the ^{1}H NMR analysis of the crude of each collection, confirming a consistent yield during the 5 h run. Additionally, ^{1}H NMR spectra of the crudes from each stage presents a very high similarity even when comparing the baselines (see Figure S2). These results show a high stability over time of the ferrofluid under harsh chemical conditions. Finally, we explored the feasibility of performing the same scale-out reaction using a solid tube reactor (see Supporting Information Section 1.5), using the exact same conditions. An increase in pressure, see Figure 3c, was detected by the pressure sensor of the Vapourtec SF-10 pump after 50 min. The pressure continued to increase, reaching 5 bar at 124 min, at which point the syringe pumps stopped due to overpressure, leading to the termination of the reaction. In contrast, no increase in pressure was observed when utilizing the liquid-walled reactor. These findings demonstrate that the liquid tube technology effectively overcomes the common challenges associated with solid handling in traditional solid tube reactors.

4. CONCLUSIONS

In conclusion, we have shown liquid-walled continuous-flow reactors that exhibit improved mixing times compared with similar solid-tube counterparts. The dependence of mixing times on flow rates, as is common in solid-tube systems, is not as pronounced for liquid-walled reactors due to the unique droplet-mixing mechanism. In using harsh lithium organometallic reagents, we did not observe degradation, nor instability of the ferrofluid walls, and continuous prolonged operation was possible, whereas the solid-tube analog reactor clogged irreversibly after only 2 h. We foresee the use of liquid-walled reactors as a universal practical solution in many other continuous flow processes that suffer from clogging due to solids such as heterogeneous catalysis or crystallization/precipitation.

■ ASSOCIATED CONTENT

Supporting Information

The Supporting Information is available free of charge at https://pubs.acs.org/doi/10.1021/acs.oprd.4c00459.

Additional experimental information, materials and methods, scale-out information, NMR spectra, X-ray images, procedures, compound characterization, and 3D-printed chamber designs (PDF)

Forced droplet generation and its resulting mixing as visualized by X-ray radiology (MP4)

■ AUTHOR INFORMATION

Corresponding Authors

Vincent Marichez − *Qfluidics, Illkirch-Graffenstaden 67400 Cedex, France*; Email: marichez@qfluidics.com

Thomas M. Hermans − *IMDEA Nanociencia, Madrid 28049, Spain; Qfluidics, Illkirch-Graffenstaden 67400 Cedex, France*; orcid.org/0000-0003-1121-1754; Email: thomas.hermans@imdea.org

Authors

Alejandro Mata − *Qfluidics, Illkirch-Graffenstaden 67400 Cedex, France*

Caroline de Fraipont − *Qfluidics, Illkirch-Graffenstaden 67400 Cedex, France*

Céline Hervieux − *Qfluidics, Illkirch-Graffenstaden 67400 Cedex, France*

Lucas Giacchetti − *Qfluidics, Illkirch-Graffenstaden 67400 Cedex, France*

Oicime Hadj-Sassi − *Qfluidics, Illkirch-Graffenstaden 67400 Cedex, France*

Alexandra Bogicevic − *Qfluidics, Illkirch-Graffenstaden 67400 Cedex, France*

Complete contact information is available at: https://pubs.acs.org/10.1021/acs.oprd.4c00459

Notes

The authors declare the following competing financial interest(s): Qfluidics provides commercial liquid-walled reactors. VM and TMH hold shares in Qfluidics.

■ ACKNOWLEDGMENTS

There are no acknowledgements.

■ REFERENCES

(1) Baumann, M.; Moody, T. S.; Smyth, M.; Wharry, S. A Perspective on Continuous Flow Chemistry in the Pharmaceutical Industry. *Org. Process Res. Dev.* **2020**, *24*, 1802−1813.

(2) Jensen, K. F. Flow chemistry—Microreaction technology comes of age. *AIChE J.* **2017**, *63*, 858−869.

(3) Ley, S. V. On Being Green: Can Flow Chemistry Help? *Chem. Rec.* **2012**, *12*, 378−390.

(4) Benison, C. H.; Payne, P. R. Manufacturing mass intensity: 15 Years of Process Mass Intensity and development of the metric into plant cleaning and beyond. *Curr. Res. Green Sustain. Chem.* **2022**, *5*, 100229.
(5) Jiménez-González, C.; Curzons, A. D.; Constable, D. J. C.; Cunningham, V. L. Expanding GSK's Solvent Selection Guide—application of life cycle assessment to enhance solvent selections. *Clean Technol. Environ. Policy* **2004**, *7*, 42−50.
(6) Noël, T.; Su, Y.; Hessel, V. Beyond Organometallic Flow Chemistry: The Principles Behind the Use of Continuous-Flow Reactors for Synthesis. In *Organometallic Flow Chemistry* Noël, T., Ed.; Springer International Publishing: Cham, 2016; pp 1−41.
(7) Sattari-Najafabadi, M.; Nasr Esfahany, M.; Wu, Z.; Sunden, B. Mass transfer between phases in microchannels: A review. *Chem. Eng. Process.* **2018**, *127*, 213−237.
(8) Movsisyan, M.; Delbeke, E. I. P.; Berton, J. K. E. T.; Battilocchio, C.; Ley, S. V.; Stevens, C. V. Taming hazardous chemistry by continuous flow technology. *Chem. Soc. Rev.* **2016**, *45*, 4892−4928.
(9) Roberge, D. M.; Ducry, L.; Bieler, N.; Cretton, P.; Zimmermann, B. Microreactor Technology: A Revolution for the Fine Chemical and Pharmaceutical Industries? *Chem. Eng. Technol.* **2005**, *28*, 318−323.
(10) Zong, J.; Yue, J. Continuous Solid Particle Flow in Microreactors for Efficient Chemical Conversion. *Ind. Eng. Chem. Res.* **2022**, *61*, 6269−6291.
(11) Dong, Z.; Zondag, S. D. A.; Schmid, M.; Wen, Z.; Noël, T. A meso-scale ultrasonic milli-reactor enables gas−liquid-solid photocatalytic reactions in flow. *Chem. Eng. J.* **2022**, *428*, 130968.
(12) Doyle, B. J.; Gutmann, B.; Bittel, M.; Hubler, T.; Macchi, A.; Roberge, D. M. Handling of Solids and Flow Characterization in a Baffleless Oscillatory Flow Coil Reactor. *Ind. Eng. Chem. Res.* **2020**, *59*, 4007−4019.
(13) Chapman, M. R.; Kwan, M. H. T.; King, G.; Jolley, K. E.; Hussain, M.; Hussain, S.; Salama, I. E.; González Niño, C.; Thompson, L. A.; Bayana, M. E.; et al. Simple and Versatile Laboratory Scale CSTR for Multiphasic Continuous-Flow Chemistry and Long Residence Times. *Org. Process Res. Dev.* **2017**, *21*, 1294−1301.
(14) Nandiwale, K. Y.; Hart, T.; Zahrt, A. F.; Nambiar, A. M. K.; Mahesh, P. T.; Mo, Y.; Nieves-Remacha, M.-J.; Johnson, M. D.; García-Losada, P.; Mateos, C.; et al. Continuous stirred-tank reactor cascade platform for self-optimization of reactions involving solids. *React. Chem. Eng.* **2022**, *7*, 1315−1327.
(15) Dunne, P.; Adachi, T.; Dev, A. A.; Sorrenti, A.; Giacchetti, L.; Bonnin, A.; Bourdon, C.; Mangin, P. H.; Coey, J. M. D.; Doudin, B.; Hermans, T. M. Liquid flow and control without solid walls. *Nature* **2020**, *581*, 58−62.
(16) Hermans, T., Coey, J. M. D., Dunne, P.; Doudin, B. Device and method for circulating liquids, EP 3351796 A1, 2018.
(17) Marichez, V.; Hermans, T.; Thebault, C. J.; Giacchetti, L. Mixing device with circulation zone and associated method, FR 3139284 A1, 2024.
(18) Dev, A. A.; Dunne, P.; Hermans, T. M.; Doudin, B. Fluid Drag Reduction by Magnetic Confinement. *Langmuir* **2022**, *38*, 719−726.
(19) Dev, A. A.; Sacarelli, F.; Bagheri, G.; Joseph, A.; Oleshkevych, A.; Bodenschatz, E.; Dunne, P.; Hermans, T.; Doudin, B. Scaling and flow profiles in magnetically confined liquid-in-liquid channels. *Top. Appl. Phys.* **2024**, *120*, 41−56.
(20) Dev, A. A.; Hermans, T. M.; Doudin, B. Ultra-Soft Liquid-Ferrofluid Interfaces. *Adv. Funct. Mater.* **2024**, *34* (48), 2411811.
(21) Yoshida, J.; Nagaki, A.; Yamada, T. Flash chemistry: fast chemical synthesis by using microreactors. *Chem.—Eur. J.* **2008**, *14*, 7450−7459.
(22) Commenge, J.-M.; Falk, L. Villermaux−Dushman protocol for experimental characterization of micromixers. *Chem. Eng. Process.* **2011**, *50*, 979−990.
(23) Arian, E.; Pauer, W. Contributions to the kinetics of the iodide−iodate test reaction for micromixing time calculation with extended incorporation models. *Chem. Eng. Sci.* **2021**, *237*, 116549.
(24) Arian, E.; Pauer, W. A comprehensive investigation of the incorporation model for micromixing time calculation. *Chem. Eng. Res. Des.* **2021**, *175*, 296−308.
(25) Haber, J.; Ausserwoeger, H.; Lehmann, C.; Pillet, L.; Schenkel, B.; Guélat, B. Minimizing Material Consumption in Flow Process Research and Development: A Novel Approach Toward Robust and Controlled Mixing of Reactants. *Org. Process Res. Dev.* **2022**, *26*, 2456−2463.
(26) Odille, F. G. J.; Stenemyr, A.; Pontén, F. Development of a Grignard-Type Reaction for Manufacturing in a Continuous-Flow Reactor. *Org. Process Res. Dev.* **2014**, *18*, 1545−1549.
(27) Kreimer, M.; Zettl, M.; Aigner, I.; Mannschott, T.; van der Wel, P.; Khinast, J. G.; Krumme, M. Performance Characterization of Static Mixers in Precipitating Environments. *Org. Process Res. Dev.* **2019**, *23*, 1308−1320.
(28) Mata, A.; Weigl, U.; Flögel, O.; Baur, P.; Hone, C. A.; Kappe, C. O. Acyl azide generation and amide bond formation in continuous-flow for the synthesis of peptides. *React. Chem. Eng.* **2020**, *5*, 645−650.
(29) Spennacchio, M.; Natho, P.; Andresini, M.; Colella, M. Continuous Flow Generation of Highly Reactive Organometallic Intermediates: A Recent Update. *J. Flow Chem.* **2024**, *14*, 43−83.
(30) Power, M.; Alcock, E.; McGlacken, G. P. Organolithium Bases in Flow Chemistry: A Review. *Org. Process Res. Dev.* **2020**, *24*, 1814−1838.

https://doi.org/10.1021/acs.oprd.4c00459
Org. Process Res. Dev. 2025, 29, 472−478